JACS
JOURNAL OF THE AMERICAN CHEMICAL SOCIETY
pubs.acs.org/JACS

Article

Merging and Clipping Nets for the Synthesis of Three- and Two-Merged Net Metal−Organic Frameworks

Yunhui Yang, Pilar Fernández-Seriñán, Borja Ortín-Rubio, Partha Samanta, Felipe Gándara, Davide M. Proserpio, Dongsik Nam, Judith Juanhuix, Inhar Imaz,* and Daniel Maspoch*

Cite This: J. Am. Chem. Soc. 2025, 147, 1344−1355

Read Online

ACCESS | Metrics & More | Article Recommendations | Supporting Information

ABSTRACT: Herein, we report how merging and clipping nets in metal−organic frameworks (MOFs) can be controlled in a single-crystal-to-single-crystal fashion using three different approaches—the merged net, clip-off chemistry, and linker reinstallation—to design and synthesize three- and two-merged net MOFs. Initially, we show the formation of three isoreticular three-merged net MOFs by linking a trimeric Sc^{3+} cluster, $Sc_3(\mu_3\text{-O})(-COO)_6$, with ditopic zigzag and tritopic linkers. The resulting MOFs exhibit three-merged edge-transitive nets—**kgd** + **hxl** + **pcu**—for the first time. Then, using these three-merged net MOFs as precursors, we selectively remove one of these subnets, the **hxl** net, via clip-off chemistry to form two-merged net MOFs. This process involves the cleavage of olefinic groups via ozonolysis, providing the resulting two-merged net MOFs with free carboxylic acid groups that can be used to tune their sorption properties such as the removal of cationic organic pollutants. Finally, we use the linker reinstallation approach to convert the two-merged net MOFs back to the three-merged net MOFs. This approach allows for the postsynthetic addition of the previously removed **hxl** merged net, enabling recovery of the initial three-merged net MOFs or synthesis of new ones using novel ditopic zigzag linkers.

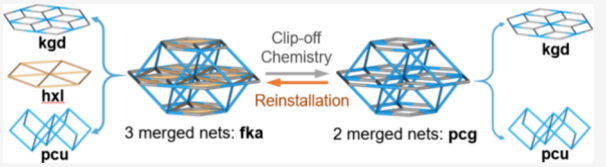

INTRODUCTION

Metal−organic frameworks (MOFs) present highly crystalline porous architectures assembled from periodically connected inorganic metal ions or clusters and organic linkers.[1] Over the past decades, the discovery, design, and synthesis of a wide range of MOF structures have been strongly linked to the implementation of reticular chemistry.[2−4] This field enables the incorporation of desired functionalities and properties into preselected organic and inorganic building blocks prior to the assembly process. These building blocks, imbued with specific geometric information and connectivity, can be reticulated according to their points of extension to align with the vertex figures of the targeted net. In this regard, edge-transitive nets with only one kind of edge are of prime importance and can be considered as ideal blueprints for rational design.[5,6] Among the approximately 100 edge-transitive nets cataloged in the Reticular Chemistry Structure Resource (RCSR) database,[7] highly connected nets with a connectivity of at least one node higher than 8 are still relatively less explored and hold significant interest. This is because their increased connectivity markedly reduces the variety of possible structures associated with different nets.[8]

Highly connected edge-transitive nets provide a unique and precise *vis-à-vis* positioning and connectivity of vertex figures, where each vertex can be considered as **net**-coded building units (**net**-cBUs) that specifically assemble into a selected net topology.[9,10] The concept to use **net**-cBUs has enabled the rational design of highly connected inorganic building blocks (e.g., polynuclear clusters) as well as branched organic linkers, ideal for constructing highly connected MOFs based on targeted net topologies. For this reason, attempted efforts have been extensively made on the use of hexanuclear $Zr_6(\mu_3\text{-O})_4(\mu_3\text{-OH})_4(-COO)_{12}$, $RE_6(\mu_3\text{-OH})_8(-COO)_{12}$, and nonanuclear $RE_9(\mu_3\text{-O})_2(\mu_3\text{-OH})_{12}(-COO)_{12}$ clusters (RE stands for rare earth), which are capable of constructing highly connected MOFs based on edge-transitive **fcu**,[11,12] **ftw**,[13,14] **shp**,[15,16] **ith**,[17] **dfs**,[18] and **alb**[10,19] nets. However, the scarcity of polynuclear clusters and the demanding synthesis of branched polycarboxylate linkers pose challenges, limiting further exploration of highly connected MOFs.

Accordingly, several innovative design strategies have emerged to intricately construct MOF structures with highly connected nets, expanding the reticular chemistry repertoire to achieve greater structural complexity. The supermolecular building block (SBB) approach demonstrates that the externally functionalized metal−organic polygons or polyhedra (MOPs) can be considered as **net**-cBUs or tertiary building units (TBUs) in MOF synthesis toward highly connected nets.[8,9,20,21] In this case, the exploration and expansion of the

Received: November 11, 2024
Revised: December 4, 2024
Accepted: December 5, 2024
Published: December 23, 2024

variety of TBUs are crucial. Notably, the **rht** and **gea** nets, based on 24-connected (24-c) **rco** MOP and 18-c **ebc** MOP, respectively, exemplify the potential of this strategy.[22,23] Another alternative strategy is the merged net approach, which allows to merge different edge-transitive nets related by symmetry into a single net, enabling the design of more intricate MOFs.[9,24−27] This approach permits the merging of distinct edge-transitive nets through shared nodes. For example, by merging two edge-transitive nets, (3,6)-c **spn** and 6-c **hxg** nets, a minimal edge-transitive net, (3,6,12)-c **sph** net, can be achieved with a higher level of complexity. This approach has been successfully applied in mixed-linker RE-MOFs, where a 12-c cuboctahedral building unit splits into two polyhedra, a 6-c hexagon and a 6-c trigonal antiprism, based on each linker.[28,29] In addition, this approach has been extended to the **spe** net based on Zr-MOFs, where two edge-transitive nets, **spn** and **epw** nets, are merged according to two distinct conformers from a single tritopic linker.[30] Although the merged net approach has been implemented in polynuclear clusters with high connectivity (RE, Zr), its application in lower nuclear clusters (e.g., the widely used paddle-wheel dimers and trimer clusters) remains largely unexplored.[27] Therefore, expanding the merged net approach to create intricate MOFs based on highly connected nets is yet challenging.

Herein, we present the synthesis and topological analysis of a three-merged net MOF constructed by connecting trimeric Sc clusters with a tritopic carboxylate linker and a ditopic zigzag carboxylate linker. This MOF exhibits one of the first examples of three distinct edge-transitive nets, **kgd** + **hxl** + **pcu**, merged within a single structure. Furthermore, we have demonstrated the synthesis of isoreticular three-merged net MOFs using alternative ditopic zigzag linkers. Leveraging this capability, we have synthesized two isoreticular three-merged net MOFs incorporating ditopic zigzag linkers containing cleavable olefinic bonds. Through the application of clip-off chemistry[31−36] to these MOFs, we have shown that one of the merged nets within the three-merged net MOFs can be detached, transforming them into novel two-merged net MOFs. Finally, we illustrate that the clipped net can be reattached to the structure via linker reinstallation, enabling the formation of three-merged net MOFs once again.

RESULTS AND DISCUSSION

Synthesis and Topological Description of BCN-31: A Three-Merged Net MOF. The trimeric carboxylate-based metal cluster, with the general formula of $M_3(\mu_3\text{-O})(-COO)_6$ (M = Fe^{3+}, Sc^{3+}, Al^{3+}, In^{3+}, Ga^{3+}, Cr^{3+}, and V^{3+}), has been one of the most explored and versatile building blocks since the early stages of this field.[20,37−39] This cluster possesses a triangular prismatic geometry that forms six connections to organic linkers. In most cases, these clusters have been interconnected through ditopic carboxylate linkers, tritopic carboxylate linkers, or a mixture of the two (Figure 1). When connected through six ditopic linkers, various MOF structures can be formed, such as MIL-101[40] with the **mtn** topology and MIL-88[41] with the **acs** topology. Conversely, when linked by six tritopic linkers, other MOF structures can be synthesized, including MIL-100[42] with the **moo** topology and InPF-110[43] with the **npo-e** topology. In contrast, when these clusters are linked by a combination of ditopic and tritopic linkers, a variety of multicomponent MOFs have been synthesized, depending on the linker ratio and arrangement. A search of the literature has shown that these clusters have been linked using three combinations of mixed ditopic and tritopic linkers: (a) two ditopic and four tritopic linkers (D:T = 1:2; e.g., PCN-285,[44] PCN-280,[44] and MIL-142A-E[45−47] with the **nht** topology), (b) three ditopic and three tritopic linkers (D:T = 1:1; e.g., MIL-143[45] with the β-cristobalite topology), and (c) four ditopic and two tritopic linkers (D:T = 2:1; e.g., MOF-907[48] with the **nha** topology) (Figure 1).

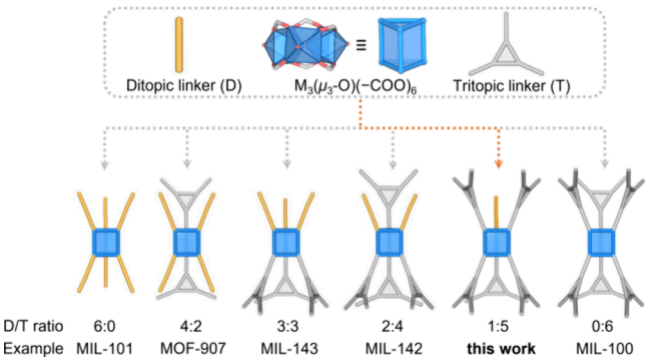

Figure 1. Illustration showing the various coordination modes of $M_3(\mu_3\text{-O})(-COO)_6$ clusters containing mixed ditopic and tritopic linkers, highlighting examples of the resulting different MOFs.

To explore the formation of MOFs with novel topologies based on these trimeric metal clusters, we decided to use a less symmetric ditopic linker to avoid topologies obtained using the typical linear ones.[49] To this end, we selected the azobenzene-3,3′-dicarboxylic acid (H_2azo), a zigzag linker with a quite large transversal width parameter of 5.7 Å, in combination with the typically used tritopic 1,3,5-tris(4-carboxyphenyl)benzene (H_3BTB) linker.[50]

Once the two organic linkers were selected, we mixed them with $Sc(NO_3)_3{\cdot}xH_2O$ in *N*,*N*-dimethylformamide (DMF) in the presence of nitric acid (HNO_3) and reacted them at 100 °C for 5 days. Following this period, we collected pure colorless hexagonal crystals. Single-crystal X-ray diffraction (SCXRD) analysis performed on these crystals revealed the formation of a 3D MOF (hereafter named as **BCN-31A**), which crystallizes in the trigonal space group *R*3*c* with corresponding unit cell parameters of $a = b = 33.706$ Å and $c = 94.078$ Å (Table S1).

The structure of **BCN-31A** is formed by 6-connected (6-c) $Sc_3(\mu_3\text{-O})(-COO)_6$ clusters, in which each Sc^{3+} cation adopts an octahedral geometry (Figure 2). Among all three Sc^{3+} cations inside the cluster, two of them are coordinated with one solvent molecule (H_2O) and the other is linked by a formate anion. The presence of formate anions can be ascribed to the decomposition of the DMF solvent during the synthesis.[43] These clusters are interconnected through five tritopic BTB linkers and one ditopic azo linker, highlighting a new linker ratio (D:T = 1:5) in this family of multicomponent MOFs (Figure S3). Connection of these clusters defines a novel metal−organic polygon, a six-membered ring, which acts as a TBU. Particularly, this ring is constructed from six $Sc_3(\mu_3\text{-O})(-COO)_6$ clusters and two bent BTB linkers. The ring is arranged in sets of two, where each set contains one bent BTB linker linked to three different $Sc_3(\mu_3\text{-O})(-COO)_6$ clusters. These two sets are interconnected by formate anions through one apical position of the $Sc_3(\mu_3\text{-O})(-COO)_6$ cluster (Figure 2b). Two BTB linkers are interlocked by strong $\pi-\pi$ interactions, with a distance of 3.67 Å between their central

https://doi.org/10.1021/jacs.4c15936
J. Am. Chem. Soc. 2025, 147, 1344−1355

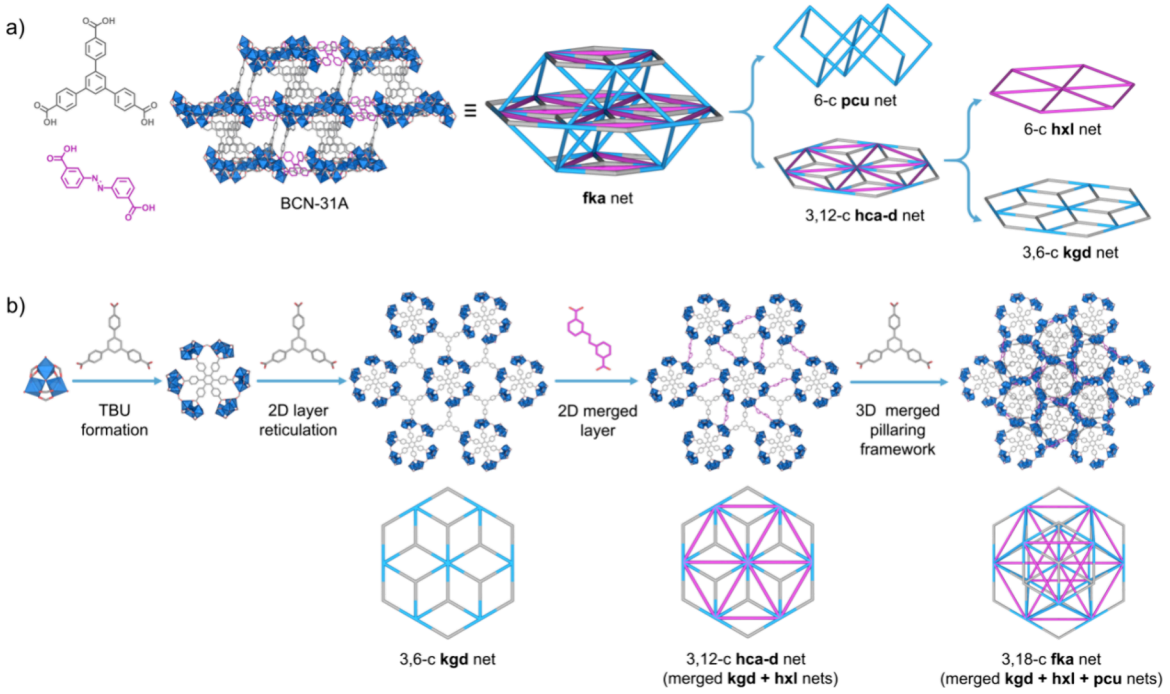

Figure 2. (a) Topological analysis of **BCN-31A** using the merged net approach. (b) Schematic illustration showing the assembly of **BCN-31A**.

aromatic rings (Figure S4). Notably, because of the bent geometry of BTB linkers, Sc^{3+} clusters from these two sets are not coplanar. Overall, this ring displays 18 points of extension, forming a flattened **egb** polyhedron isoreticular to J_{36} Johnson-type elongated triangular gyrobicupola (Figure S5).

Based on this simplification, the entire structure of **BCN-31A** revealed the formation of a novel (3,18)-c underlying net, where 18-c TBUs are connected by mixed linkers to form a three-periodic structure. To study and understand the assembly of **BCN-31A**, we conducted a topological analysis, disentangling this highly connected net based on the symmetry of each linker. Specifically, **BCN-31A** can be deconstructed into two-periodic layers pillared by BTB linkers. Within the two-periodic structure, each TBU is linked by six azo and six BTB linkers, presenting a partially 12-c dodecagonal TBU. The azo linker exhibits a *trans* conformation, adopting a zigzag geometry. Further topological analysis of this two-periodic layer subnet unveiled that this layer displays as the dual of the **hca** net: the (3,12)-c **hca-d** net (Figure S6). Indeed, the merged net approach can also be employed to describe this substructure. The underlying net of this two-periodic layer can be further deconstructed into two distinctive topologies, edge-transitive **hxl** and **kgd** nets derived from the azo and BTB linkers, respectively.

These two-periodic layers are further pillared by 12 BTB linkers to form a three-periodic structure. Among these 12 pillared BTB linkers, each of two pairs is doubly bridging to the same TBU, resulting in an overall TBU connectivity of 18 from which 12 are in-plane and 6 pillaring (Figure S7). Consequently, considering solely the pillaring of this 6-c TBU, the underlying net reveals the **pcu** topology. Overall, **BCN-31A** presents the first example of three distinct edge-transitive nets merged: **kgd** + **hxl** + **pcu** (Figure 2a), where the 18-c TBU arises from the juxtaposition of both 6-c hexagonal and 6-c octahedral nodes, respectively (Figure S8). By analyzing the underlying topology, the resulting structure displays a (3,18)-c binodal **fka** net based on this distinctive 18-c TBU (Table S2). While this net was cataloged in the RCSR database, it is the first time that it has been experimentally achieved.[51] This discovery marks the first case of three nets merged by using a mixed-linker strategy.

Finally, the phase purity of **BCN-31A** was validated by powder X-ray diffraction (PXRD), and the proton nuclear magnetic resonance (^{1}H NMR) spectrum of the digested sample confirmed the expected BTB and azo ratio of 10:3 (Figures S9 and S10). Thus, the charge-balanced chemical formula of **BCN-31A** determined by SCXRD and elemental analysis is $[Sc_3O(H_2O)_2(BTB)_{5/3}(azo)_{1/2}(HCOO)_{1/2}](NO_3)_{1/2}\cdot(solv)_x$. Nitrogen sorption measurements on **BCN-31A** proved its microporosity, showing a Brunauer–Emmett–Teller surface area (S_{BET}) of up to 1796 $m^2\ g^{-1}$ (Figure S11). The pore size distribution (PSD) revealed a main pore population of ca. 10 Å and a minor population of ca. 7 Å, attributed to the intrinsic porosity of the framework (Figure S12).

Clipping a Net from the Three-Merged Net BCN-31B: Synthesis of a New Two-Merged Net BCN-32. Once the first three-merged net MOF was synthesized, we explored whether clip-off chemistry could be used to disconnect one of these three nets, thus enabling the synthesis of a new two-merged net MOF. For this purpose, we replaced the ditopic H_2azo linker, which lacks any cleavable olefin bond, with the alkene-containing 3,3′-stilbenedicarboxylic acid (H_2sti) linker. With this change, we hypothesized that the 3D three-merged (**kgd** + **hxl** + **pcu**) net **BCN-31B** (isoreticular to **BCN-31A**) would convert into a new 3D two-merged (**kgd** + **pcu**) net MOF (hereafter named as **BCN-32**), as the new ditopic linkers are located at the crystallographic positions corresponding to the **hxl** net.

In a first step, **BCN-31B** was synthesized by reacting a DMF solution containing $Sc(NO_3)_3\cdot xH_2O$, H_3BTB, H_2sti, and HNO_3 at 100 °C for 5 days. SCXRD confirmed the formation of **BCN-31B** (Figure 3a), isoreticular to **BCN-31A**, which crystallizes in a trigonal lattice with the *R*3*c* space group and

https://doi.org/10.1021/jacs.4c15936
J. Am. Chem. Soc. 2025, 147, 1344−1355

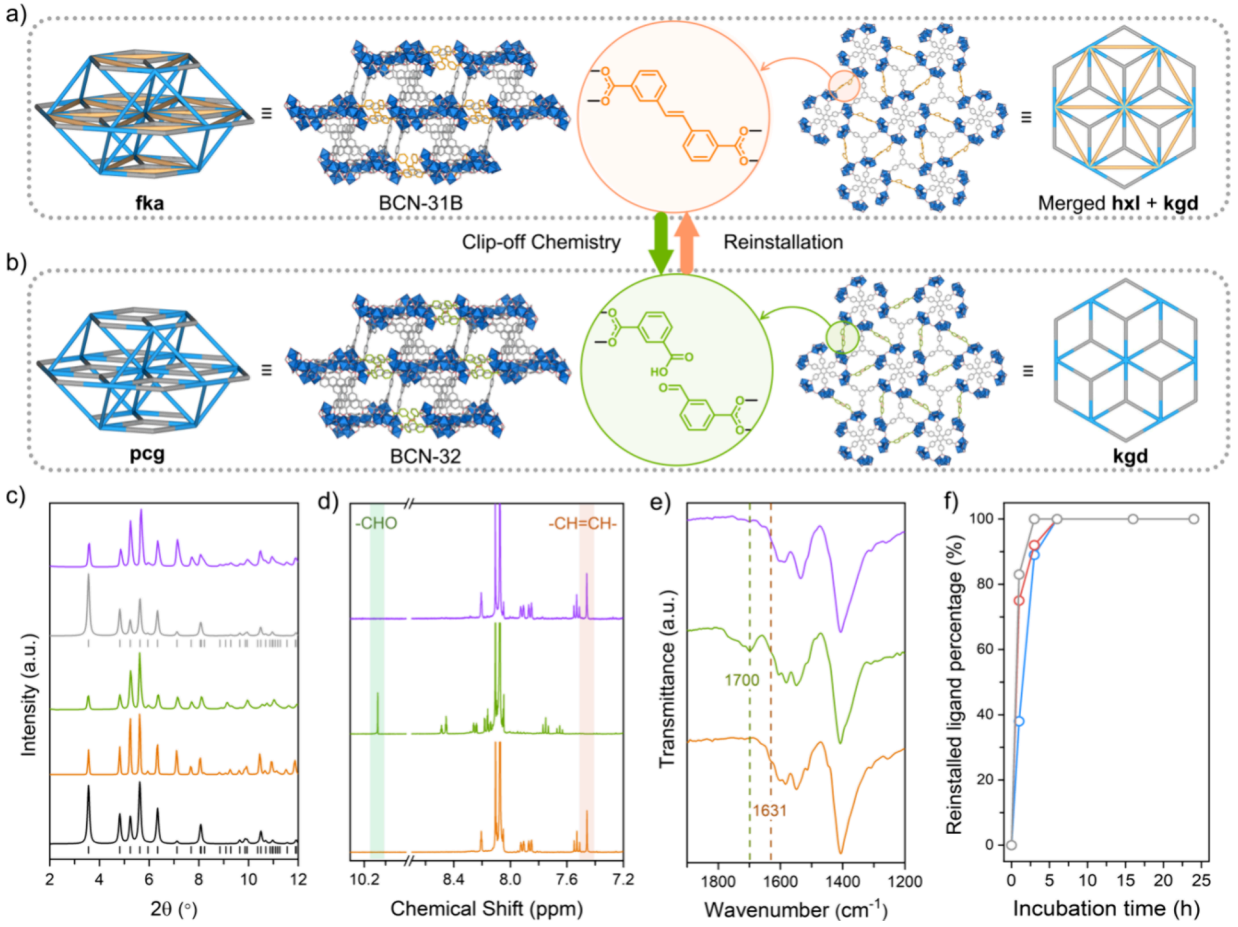

Figure 3. (a) Structure of **BCN-31B** and its related topology. (b) Structure of **BCN-32** and its related topology. (c) PXRD of simulated **BCN-31B** (black), experimental **BCN-31B** (orange), experimental **BCN-32** (green), simulated **BCN-32** (gray), and experimental **BCN-31B** obtained after linker reinstallation (purple). The vertical lines shown below two simulated PXRD patterns are Bragg positions based on the corresponding single-crystal structures. (d) ^{1}H NMR spectra of **BCN-31B** (orange), **BCN-32** (green), and **BCN-31B** obtained after linker reinstallation (purple). The protons from olefinic bonds and aldehyde groups are highlighted in orange and green, respectively. (e) FTIR spectra of **BCN-31B** (orange), **BCN-32** (green), and **BCN-31B** obtained after linker reinstallation (purple). (f) Ratio of reinstalled sti linkers in **BCN-32** as a function of incubation time at different concentrations of sti solutions based on ^{1}H NMR studies: 2.5 mM (blue), 5 mM (red), and 10 mM (gray).

the corresponding unit cell parameters of $a = b = 33.674$ Å and $c = 94.193$ Å (Table S3). In this case, PXRD also confirmed its phase purity (Figure 3c and Figure S13), and the ^{1}H NMR spectrum of the digested sample confirmed the expected BTB and sti ratio of 10:3 (Figure S14). As expected, the N_2 sorption isotherm collected at 77 K for **BCN-31B** confirmed an S_{BET} of 1730 $m^2\ g^{-1}$ (Figure S15) and a pore size distribution similar to that of **BCN-31A** (ca. 7 and 10 Å, Figure S16).

Next, we performed a solid−gas ozonolysis reaction to cleave the olefinic bond of the sti linkers. To begin with, 20 mg of **BCN-31B**, previously soaked in a THF solvent and air-dried, was packed into a plastic tube and connected to the ozonator setup. Then, dry ozone was flowed (~15 g Nm^{-3}) continuously through the sample for 2.5 min. The ozonized sample, namely **BCN-32**, maintained the hexagonal crystal shape and could be analyzed by SCXRD. SCXRD analysis showed that **BCN-32** crystallizes in a trigonal crystal system with the *R*3*c* space group with the corresponding lattice parameters of $a = b = 33.706$ Å and $c = 94.075$ Å (Table S4). Overall, **BCN-32** exhibits a related 3D structure to that of **BCN-31B** but with evident changes in its components (Figure 3b). Indeed, SCXRD data confirmed the integrity of the TBUs and of the BTB linkers. However, sti linkers initially located in **BCN-31B** could no longer be precisely refined as electron density maps revealed positional disorder in the carbon atoms of the phenyl rings in **BCN-32**, suggesting the cleavage of sti linkers.

To further validate the complete cleavage of all olefinic bonds of sti linkers, we analyzed a digested **BCN-32** sample by ^{1}H NMR and compared the resulting spectrum to that of the starting **BCN-31B** (Figure 3d and Figures S17 and S18). The ^{1}H NMR spectrum of **BCN-31B** showed the characteristic peak of the olefinic protons of sti at $\delta = 7.46$ ppm. In contrast, the spectrum of the digested **BCN-32** corroborated the disappearance of this olefinic signal. Furthermore, this later spectrum also revealed the disappearance of the phenyl protons ($\delta = 8.21$, 7.92, 7.86, and 7.53 ppm) of the sti but did show the characteristic signals for the isophthalic acid (*m*-BDC, phenyl protons at $\delta = 8.49$, 8.16, and 7.75 ppm) and 3-formylbenzoate (3-FBA, phenyl protons at $\delta = 8.45$, 8.25, and 7.65 ppm). This integrated spectrum indicated a proton ratio corresponding to *m*-BDC/3-FBA of 1:1. Accordingly, these results showed that sti linkers had been quantitatively cleaved through ozonolysis and subsequently converted into mono-coordinated linkers: a single deprotonated isophthalic acid (*m*-BDC) and 3-formylbenzoate (3-FBA). Supporting this

https://doi.org/10.1021/jacs.4c15936
J. Am. Chem. Soc. 2025, 147, 1344−1355

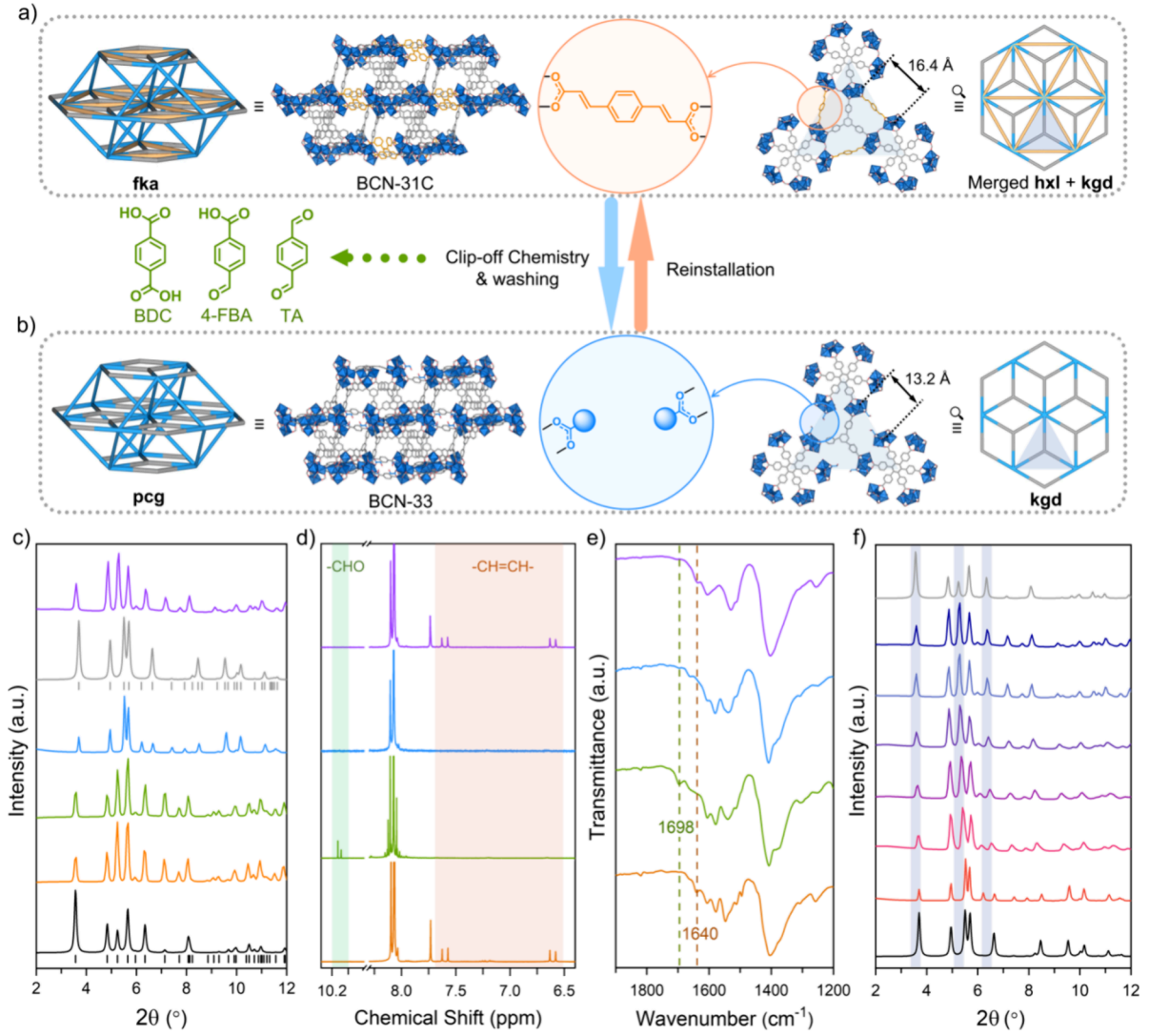

Figure 4. (a) Structure of **BCN-31C** and its related topology. (b) Structure of **BCN-33** and its related topology. (c) PXRD of simulated **BCN-31C** (black), experimental **BCN-31C** (orange), ozonized **BCN-31C** (green), experimental **BCN-33** obtained after washing with DMF (blue), simulated **BCN-33** (gray), and experimental **BCN-31C** after linker reinstallation from **BCN-33** (purple). The vertical lines shown below two simulated PXRD patterns are Bragg positions based on the corresponding single-crystal structures. (d) ^{1}H NMR spectra of **BCN-31C** (orange), ozonized **BCN-31C** (green), **BCN-33** obtained after washing with DMF (blue), and **BCN-31C** after linker reinstallation from **BCN-33** (purple). The protons from olefinic bonds and aldehyde groups are highlighted in orange and green, respectively. (e) FTIR of **BCN-31C** (orange), ozonized **BCN-31C** (green), **BCN-33** obtained after washing with DMF (blue), and **BCN-31C** obtained after linker installation from **BCN-33** (purple). (f) Evolution of the linker reinstallation process (pdac concentration: 2.5 mM) in **BCN-33** followed by PXRD, showing a gradual structural expansion during this process: simulated **BCN-33** (black), experimental **BCN-33** (orange), **BCN-33** exposed to pdac at different incubation times (incubation times of 1, 3, 6, 16, and 24 h from red to dark blue), and simulated **BCN-31C** (gray).

oxidative cleavage reaction, the Fourier-transform infrared (FTIR) spectrum of **BCN-32** confirmed that the characteristic band of olefinic groups at 1631 cm^{-1} had disappeared, in quite contrast with that shown for the pristine **BCN-31B** (Figure 3e and Figure S19). In addition, a more intense band at 1700 cm^{-1} corresponding to the carbonyl groups was largely enhanced, which is in accordance with the generation of aldehyde and free carboxylic acid groups from ozonized products.[31] The PXRD pattern of **BCN-32** matched well with the one calculated from the crystal structure, confirming that the cleavage of alkene bonds via ozonolysis did not compromise the crystallinity throughout the bulk sample (Figure 3c and Figure S20). The N_2 sorption isotherm collected at 77 K for **BCN-32** confirmed an S_{BET} of 1490 m^2 g^{-1} (Figure S21). Additionally, the PSD of **BCN-32** showed pore sizes comparable to those of **BCN-31B** (ca. 7 and 10 Å, Figure S22).

Topologically, the cleavage of sti linkers affects directly the underlying net of **BCN-32** by decreasing the connectivity of the 18-c TBU to 12. This confirms that one of the three-merged nets from **BCN-31B**, the **hxl** net, has been entirely removed. As a result, the overall framework of **BCN-32** presents the new underlying (3,12)-c **pcg** topology, resulting from merging the **pcu** and **kgd** nets ("**pc**" from **pcu** and "**g**" from **kgd**), which was already included in the RCSR database but that was only theoretically predicted (Figure 3b).[52]

Switching the Formation Back from the Two-Merged Net BCN-32 to the Three-Merged Net BCN-31B via Linker Reinstallation. After confirming the possibility to remove the **hxl** subnet from **BCN-31B** to form the two-merged

https://doi.org/10.1021/jacs.4c15936
J. Am. Chem. Soc. 2025, 147, 1344−1355

net **BCN-32**, we sought to reinstall this cleaved subnet to form again **BCN-31B** via linker reinstallation. In other words, we sought to synthesize a three-merged net MOF from a two-merged net MOF via linker reinstallation.

To this end, **BCN-32** was immersed in a 10 mL of DMF solution containing H_2sti at 65 °C. The effects of incubation time and H_2sti concentration in DMF solution were systematically studied. The linker reinstallation process was monitored and quantified based on the ratio between BTB and sti from ^{1}H NMR of the digested samples (Figures S23–S25). We initially examined the linker reinstallation process with a H_2sti concentration of 2.5 mM in DMF solution. As shown in Figure 3f, the sti content increased dramatically within the first hour (about 40%) reaching its maximum after 6 h, indicating the complete reinstallation of sti linkers. When the concentration of H_2sti linkers was increased to 5 and 10 mM, the linker reinstallation process was slightly accelerated, reaching the maximum sti linker content within 3 h. Within all this transformation process, the crystallinity of the samples remained, with the PXRD pattern of the new **BCN-31B** matching well with that of the pristine **BCN-31B** (Figures S26–S28). This linker reinstallation could also be confirmed by FTIR, which showed the appearance of the characteristic band of the olefinic bond at 1631 cm^{-1} and the attenuation of the band of the carbonyl groups at 1700 cm^{-1} (Figure 3e and Figure S19). Furthermore, the porosity of the fully linker-reinstalled **BCN-31B** (incubation time: 24 h) was confirmed by N_2 adsorption, exhibiting an S_{BET} of 1007 m^2 g^{-1} (Figure S29). The PSD of this sample showed pore sizes comparable to those of **BCN-32** or **BCN-31B** (ca. 7 and 10 Å, Figure S30).

Expanding the Synthesis of Three- and Two-Merged Net MOFs. Encouraged by these results, we sought to further explore the use of another cleavable linker to form another isoreticular three-merged net MOF (hereafter called **BCN-31C**) and its conversion to the two-merged net **BCN-33** via clip-off chemistry. To do this, we chose 1,4-phenylene diacrylic acid (H_2pdac) as our second cleavable linker because it can also adopt a zigzag geometry, the distance between its two carboxylate moieties is similar to that shown by the sti linker, and it contains two olefinic bonds alongside with a phenylene group. Thus, its oxidative cleavage will release the central phenyl ring leaving an empty space inside the structure.

Colorless octahedral crystals of **BCN-31C** were obtained following similar synthetic conditions to those previously used for **BCN-31A** and **BCN-31B**. SCXRD analysis of these crystals successfully confirmed the formation of a novel isoreticular three-merged net MOF (Figure 4a and Table S5). Phase purity of this sample was confirmed by PXRD and ^{1}H NMR of the digested sample (Figure 4c,d and Figures S31 and S32), which showed the expected ratio of BTB and pdac linkers of 10:3. N_2 sorption experiments at 77 K for **BCN-31C** confirmed its microporosity, with an S_{BET} of 1733 m^2 g^{-1} (Figure S33) and pore sizes comparable to those of **BCN-31A** or **BCN-31B** (ca. 10 and 7 Å, Figure S34).

Then, **BCN-31C** was also used as the precursor to synthesize a new two-merged net MOF called **BCN-33** by removing the **hxl** subnet using clip-off chemistry. Briefly, crystals of **BCN-31C** were exposed under dry ozone flow (ozone concentration of 15 g/g Nm^{-3}) for 3 min. PXRD analysis of the ozonized sample revealed a similar crystalline pattern to that of the pristine **BCN-31C** (Figure 4c). On the other hand, the ^{1}H NMR spectrum of the digested ozonized sample demonstrated that the signals at 6.6 and 7.6 ppm corresponding to the olefinic protons totally disappeared, indicating the complete cleavage of the pdac linkers (Figure 4d and Figure S35). This spectrum further indicated that the central phenylene group of the pdac linker was disconnected from the structure in the form of the expected three aromatic molecules resulting from the ozonolysis: terephthalic acid (BDC), 4-formylbenzoic acid (4-FBA), and terephthaldehyde (TA). Moreover, FTIR confirmed the disappearance of the band at 1640 cm^{-1} corresponding to the olefinic groups, whereas the band at 1698 cm^{-1} corresponding to the carbonyl groups got largely enhanced, which is in accordance with the generation of aldehyde and free carboxylic acid groups from ozonized products (Figure 4e and Figure S36).

Note here that, if one analyzes the connectivity and PXRD of this ozonized sample, we can consider it identical to **BCN-32** (Figure S37). The only difference between this ozonized sample and the previous **BCN-32** is their monocoordinated linkers that results from cleaving sti or pdac using ozonolysis. While a mixture of a single deprotonated isophthalic acid and 3-formylbenzoate is composed of **BCN-32** coming from the cleavage of **BCN-31B**, the structure resulting from the cleavage of **BCN-31C** is composed of a mixture of monocoordinated single deprotonated oxalic acid and glyoxylate together with the detached BDC, 4-FBA, and TA.

However, this structure slightly changes after removing the free BDC, 4-FBA, and TA guest molecules. Indeed, the removal of these guest molecules results in a slight contraction of the structure forming a contracted version of **BCN-32** (hereafter called **BCN-33**, Figure 4b). The removal of these detached aromatic guests was achieved by washing the ozonized crystals with hot DMF at 65 °C for 3 days. During this period, the supernatant was replaced with fresh DMF every 8 h. The first evidence of the complete removal of these guest molecules was provided by ^{1}H NMR of the digested **BCN-33**, which showed that all peaks coming from the free aromatic products including BDC, 4-FBA, and TA were eliminated through the washing process, and only the peaks corresponding to the BTB linker were preserved (Figure 4d and Figure S38). In addition, FTIR showed that the band of **BCN-33** at 1698 cm^{-1} corresponding to the carbonyl groups was significantly attenuated, identical to that of the pristine **BCN-31**, which further confirmed the successful removal of BDC, 4-FBA, and TA (Figure 4e and Figure S36).

Remarkably, the single-crystal character of **BCN-33** was preserved throughout all these treatments, allowing SCXRD to be used to determine its crystal structure. **BCN-33** crystallizes in the trigonal crystal system with the centrosymmetric $R\bar{3}c$ space group, with corresponding lattice parameters of $a = b =$ 32.096 Å and $c = 93.026$ Å (Table S6). This structure confirms the formation of the expected two-merged net MOF, built up from connecting the trimeric Sc clusters through BTB linkers (Figure 4b). It also reveals the presence of monocoordinated glyoxylate/oxalate linkers (although SCXRD data quality did not allow perfect distinction between them). Additionally, no free aromatic residues from the ozonized pdac linker could be located anymore, as no residual electron density was found crystallographically.

The structure of **BCN-33** clearly shows the slight structural contraction that occurs after removing the detached BDC, 4-FBA, and TA. In **BCN-31C**, the distance of the two trimeric Sc clusters bridged by the pdac linker is 16.4 Å (measured between the two central O atoms of the cluster). This distance is very similar to **BCN-32** (17.1 Å). However, in **BCN-33**, this

https://doi.org/10.1021/jacs.4c15936
J. Am. Chem. Soc. 2025, 147, 1344–1355

relative distance has decreased to 13.2 Å (Figure 4a,b and Figure S39). This contraction of the framework was also corroborated by PXRD, particularly affecting the crystallographic plane perpendicular to the layer containing the cleavable linkers (i.e., the two-periodic layers) in **BCN-31C**. For example, the diffraction peak of **BCN-31C** or **BCN-32** at 2θ = 5.2° corresponding to the $(2\bar{1}0)$ crystallographic plane, which is perpendicular to the two-periodic layer, shifted to a higher angle at 2θ = 5.5° in the same plane of **BCN-33**, resulting in a decrease in the *d*-spacing from 1.68 to 1.60 nm, indicative of interplanar spacing compression (Figure 4c and Figure S40). This observation is also consistent with the single-crystal data, where the unit cell volume suggested that the framework contraction is about 10%. For this MOF, N_2 sorption experiments at 77 K also confirmed its microporosity, with a decrease in the S_{BET} down to 1331 $m^2\ g^{-1}$ (Figure S41) and pore sizes (ca. 10 and 7 Å) comparable to **BCN-31C** (Figure S42).

Finally, following a similar linker reinstallation process, we studied if the three-merged net **BCN-31C** could be reconstituted by incubating **BCN-33** in various concentrations of H_2pdac in DMF solution at 65 °C for different periods of time. The linker reinstallation percentage was determined and calculated based on the ratio between H_3BTB and H_2pdac from ^{1}H NMR results of the digested samples (Figures S43–45). To begin with, we investigated the linker reinstallation process when the H_2pdac concentration was set to 2.5 mM. Under these conditions, the pdac content in **BCN-33** increased significantly within the first hour (about 50%) and stabilized after 16 h, indicating that pdac linkers have been fully reinstalled reconstituting **BCN-31C**. Then, we systematically studied the linker reinstallation process by increasing the concentration of H_2pdac linker to 5 and 10 mM, confirming that pdac linkers could be installed more rapidly and reach to the maximum content after 6 h under these conditions (Figure S46).

Given the distinct difference in PXRD patterns between the three-merged net **BCN-31C** and the two-merged net **BCN-33**, we could confirm the completeness of linker reinstallation by PXRD (Figure 4c). For the concentration of H_2pdac in DMF solution at 2.5 mM, a gradual and continuous phase transition from **BCN-33** to **BCN-31C** was observed over different incubation times. For example, the diffraction peak of **BCN-33** at 2θ = 5.5° corresponding to the $(2\bar{1}0)$ crystallographic plane gradually shifted back into a lower angle at 2θ = 5.2°, which is associated with the same plane of **BCN-31C** after 16 h. Throughout the process, all MOF samples remained crystalline and there were no extra peaks found, indicating a homogeneous phase transition throughout the entire bulk sample (Figure 4f and Figures S47–S49). This is rarely observed in the linker reinstallation process in MOFs, as many reported examples could not follow PXRD by different incubation times or showed the appearance of two phases coexisting during the linker reinstallation process.[53−60] Moreover, after the complete linker reinstallation, the FTIR spectrum showed the reappearance of the characteristic band at 1640 cm^{-1} corresponding to the olefinic bond (Figure 4e and Figure S36). Moreover, the porosity of the fully linker-reinstalled **BCN-31C** (incubation time: 24 h) was confirmed by N_2 adsorption, with an S_{BET} of 1403 $m^2\ g^{-1}$ (Figure S50). The PSD of this sample showed pore sizes comparable to **BCN-31C** (ca. 7 and 10 Å, Figure S51).

Inspired by this net reinstallation process and the easy monitoring by PXRD, we endeavored to explore the incorporation of an alternative ditopic linker having a different length compared to pdac (Figure 5a). This exploration could lead to the formation of novel three-merged net MOFs, isoreticular to **BCN-31A-C**. Specifically, we selected biphenyl-3,3′-dicarboxylic acid (H_2bpdc) as the new ditopic linker. To install it, we incubated **BCN-33** with a DMF solution of H_2bpdc at a concentration of 2.5 mM for 24 h followed by thorough washing with fresh DMF. The PXRD pattern of the

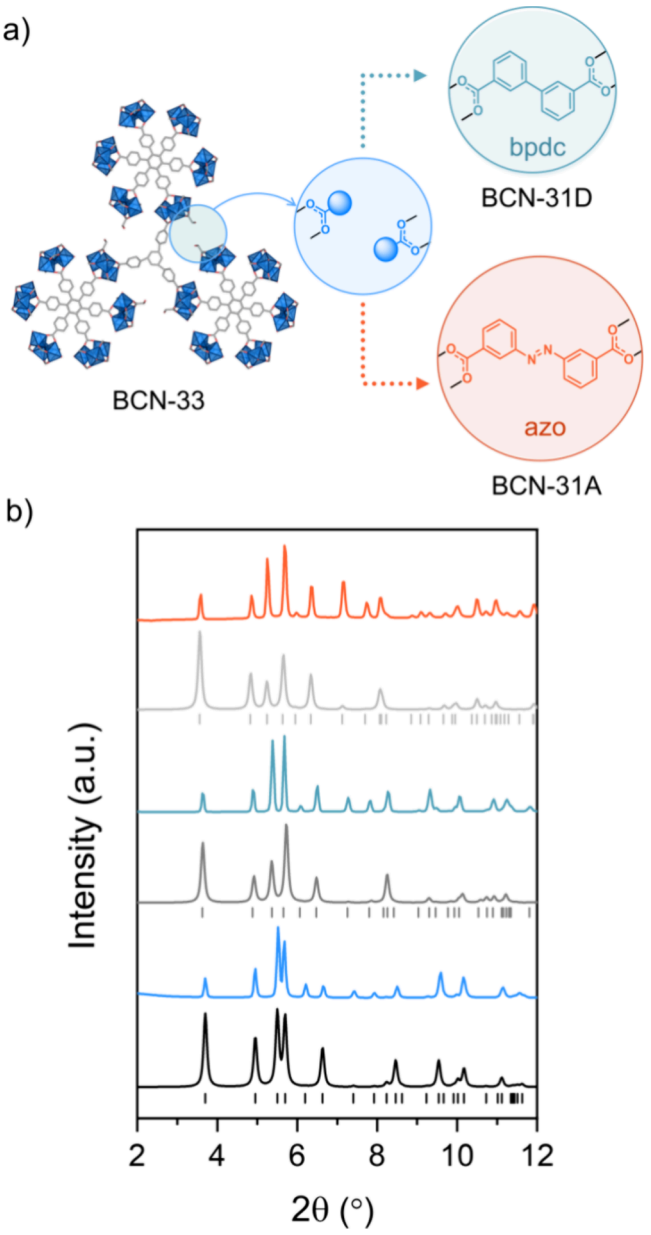

Figure 5. (a) Scheme of the installation of bpdc and azo in **BCN-33**. (b) PXRD patterns of simulated **BCN-33** (black), experimental **BCN-33** (blue), simulated **BCN-31D** (gray), experimental **BCN-31D** after bpdc installation (cyan), simulated **BCN-31A** (light gray), and experimental **BCN-31A** after azo installation (red). The vertical lines shown below simulated PXRD patterns of **BCN-33** and **BCN-31A** are Bragg positions based on the corresponding single-crystal structures. Similarly, the vertical lines shown below simulated PXRD patterns of **BCN-31D** are Bragg positions based on the structure modeling.

https://doi.org/10.1021/jacs.4c15936
J. Am. Chem. Soc. 2025, 147, 1344−1355

resulting crystals showed clear differences in diffraction peaks compared to those of **BCN-33** (Figure 5b, Figure S52, and Table S7). For instance, the characteristic peak of **BCN-33** at 2θ = 5.5° shifted to a lower angle at 2θ = 5.38° after 24 h, consistent with the simulated pattern derived from the isoreticular structure containing both BTB and bpdc linkers (hereafter referred to as **BCN-31D**). This structure was built and geometrically optimized by using the Materials Studio Forcite module.[61] Additionally, ^{1}H NMR spectra of the digested **BCN-31D** further confirmed the successful incorporation of the bpdc linker (Figure S53). N_2 sorption experiments at 77 K confirmed the accessible porosity of **BCN-31D**, with an S_{BET} of 938 m^2 g^{-1} (Figure S54) and pore sizes comparable to **BCN-31A-C** (Figure S55).

Finally, to complete the series of transformations, we incubated **BCN-33** with a DMF solution of H_2azo at a concentration of 2.5 mM for 24 h, aiming to synthesize the initial **BCN-31A**. Interestingly, both PXRD and ^{1}H NMR spectra of the digested samples confirmed the successful formation of **BCN-31A** (Figures S56 and S57). Specifically, PXRD revealed that the characteristic peak of **BCN-33** at 2θ = 5.5° shifted to a lower angle at 2θ = 5.25° after 24 h (Figure 5b), aligning with the simulated pattern obtained from the single-crystal structure of **BCN-31A**. The porosity of the fully azo linker-reinstalled **BCN-31A** was studied by N_2 adsorption at 77 K, showing an S_{BET} of 1350 m^2 g^{-1} (Figure S58) and pore sizes similar to those of as-made **BCN-31A** (Figure S59).

Exploiting the Generation of Free Carboxylic Acid Groups during the Cleavage of Olefinic Bonds in MOFs to Capture Cationic Species. Apart from structural transformations, clip-off chemistry can be used to introduce new functionalities within the resulting frameworks. For instance, in this study, when the olefinic bonds of the three-merged net **BCN-31B** and **BCN-31C** are cleaved through ozonolysis, aldehyde (−CHO) and carboxylic acid (−COOH) groups are generated and remain free in the resulting two-merged net **BCN-32** and **BCN-33**. Accordingly, we aimed to explore the potential of these free carboxylic acid groups for capturing emerging cationic organic contaminants from water. This approach is motivated by the well-known ability of free carboxylic acid groups in MOFs to interact strongly with cationic species through electrostatic interactions or with amine groups via hydrogen bonding.[62−64]

In this regard, we selected methylene blue (MB), crystal violet (CV), and rhodamine B (RhB) as our cationic dye pollutants because they differ in size and contain tertiary amine functionalities. Subsequently, 10 mg of each of the four MOFs was incubated in a 10 ppm solution of each dye, and the adsorption process was monitored with UV−vis spectroscopy at different time intervals (Figure 6). When comparing the capture performance of both **BCN-31B** and **BCN-32**, we first observed that **BCN-31B** exhibits a rapid removal of MB, and it reaches saturation with a maximum capacity of 9.9 mg g^{-1} in 110 min. In contrast, **BCN-32** showed a relatively slower rate for the MB removal, and in 110 min, it reached a capacity of 6.3 mg g^{-1} (Figure 6a and Figure S61). After 210 min of incubation time, the capture of MB with **BCN-32** reached saturation with a maximum capacity of 8.5 mg g^{-1}. This difference in efficiency of **BCN-31B** and **BCN-32** can be attributed to the surface area of the respective adsorbents. Since the surface area is higher in the case of **BCN-31B** (1730 m^2 g^{-1}) as compared to **BCN-32** (1490 m^2 g^{-1}), a better efficiency in capture of MB was obtained for **BCN-31B**. In

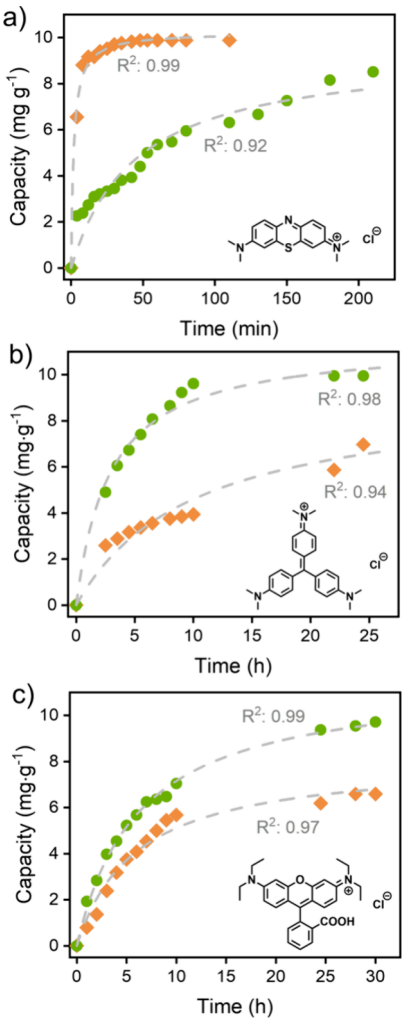

Figure 6. Adsorption kinetics for the capture of (a) methylene blue (MB), (b) crystal violet (CV), and (c) rhodamine B (RhB), each at an initial concentration of 10 ppm, by **BCN-31B** (orange) and **BCN-32** (green) fitted in a pseudo-second-order kinetic model.

contrast to this observation with MB, a completely reverse trend was observed in the case of bulkier organic dyes, i.e., CV and RhB. When the removal of CV was performed with **BCN-32**, it reached saturation in 24 h with a maximum capacity of 9.95 mg g^{-1}. Meanwhile, after the same incubation time, the parent MOF (**BCN-31B**) demonstrated comparatively lower efficiency with a capacity of 6.97 mg g^{-1} (Figure 6b and Figure S62). However, the difference in performance became even higher in the case of RhB, where **BCN-32** exhibited 31% higher removal efficiency over **BCN-31B** (Figure S63). The capacity of **BCN-32** for the capture of RhB reached its maximum after 30 h of incubation, and it was determined to be 9.7 mg g^{-1} (Figure 6c). On the other hand, after the same time period, the capacity of **BCN-31B** was found to be only 6.6 mg g^{-1}. Therefore, we clearly observed a superior performance for **BCN-32**, which is functionalized with free carboxylic acid groups, over the parent **BCN-31B** for the removal of bulkier cationic organic pollutants (CV and RhB), where the equilibrium time was comparatively higher. Moreover, the kinetics (capacity versus time study) for this sorption process in each case was found to follow the pseudo-second-order model. This observation indicated that the adsorption process included interactions between the adsorbate molecules and the

https://doi.org/10.1021/jacs.4c15936
J. Am. Chem. Soc. 2025, 147, 1344−1355

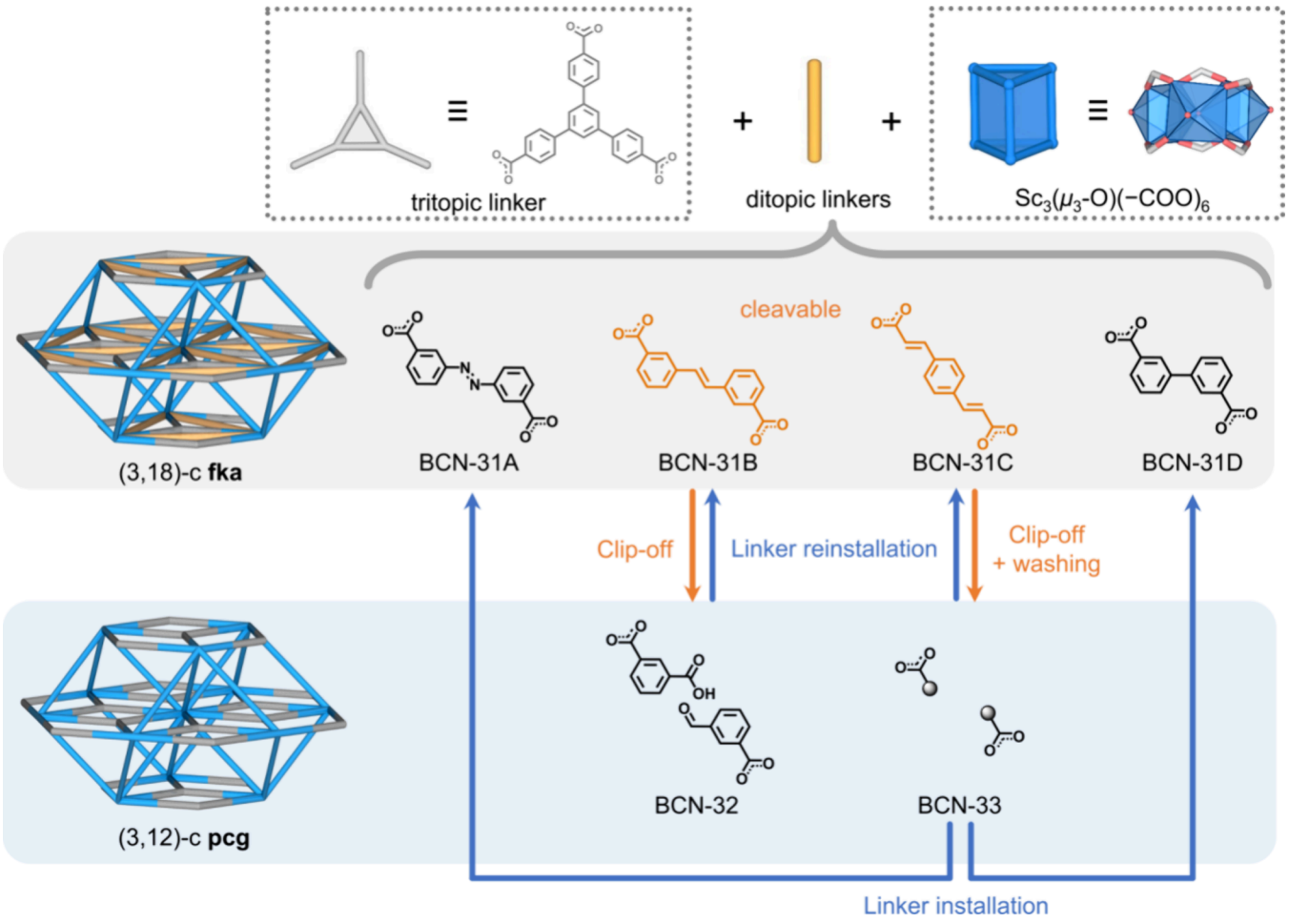

Figure 7. Comprehensive scheme showing various approaches used in this work: the merged net, clip-off chemistry, and linker reinstallation.

adsorbent. Consequently, the interaction between the generated free carboxylic acid groups in **BCN-32** after the ozonolysis process and cationic dyes plays a significant role in the capture process.

Enthused by this result, we expanded this study using both **BCN-31C** and **BCN-33** as adsorbents. Interestingly, for each cationic dye (MB, CV, and RhB), the removal study using these two MOFs showed a similar tendency to that of **BCN-31B** and **BCN-32**, confirming the positive effect of the free carboxylic groups generated by ozonolysis. In the case of MB removal, **BCN-31C** demonstrated comparatively higher performance with a maximum capacity of 9.9 mg g^{-1} (in 3 h) over **BCN-33** (capacity of 9.2 mg g^{-1} in 3 h; Figures S64 and S65). However, in the case of CV and RhB, **BCN-33** exhibited a higher capture efficiency as compared to **BCN-31C**. For the removal of CV with **BCN-33**, saturation was reached in 24 h with a maximum capacity of 9.8 mg g^{-1}. However, after the same incubation time, **BCN-31C** exhibited a lower capacity of only 7.8 mg g^{-1} (Figures S66 and S67). Again, the difference in the performance became even higher in the case of RhB, where **BCN-33** showed 45% higher efficiency over **BCN-31C** (Figures S68 and S69). The capacity of **BCN-31C** for the RhB dye capture was found to be only 5.2 mg g^{-1} in a time duration of 30 h, while **BCN-33** showed a maximum capacity of 9.8 mg g^{-1} in 28 h. Therefore, similar to **BCN-32**, in the case of **BCN-33**, the functional groups directed toward the higher efficiency in the capture of bulkier cationic dyes (CV and RhB). Moreover, the good correlation between the experimental kinetic plot (capacity versus time study) and the pseudo-second-order kinetic model further affirmed that the removal process included various interactions between the adsorbate molecules and the adsorbent. Furthermore, the structural integrity of each MOF was retained even after the dye capture study, and it was affirmed by the PXRD patterns of each solid (Figures S70−S73).

CONCLUSIONS

We have demonstrated the synthesis of three isoreticular three-merged net MOFs (**BCN-31A-C**) by connecting the typical trimeric Sc cluster through tritopic and ditopic zigzag linkers. The underlying net of these MOFs results, for the first time, from three-merged edge-transitive nets: **kgd** + **hxl** + **pcu** (**fka**). This discovery opens avenues for designing intricate MOF structures based on multiple edge-transitive nets. Utilizing these three-merged net MOFs as precursors, we have also showcased the synthesis of two-merged net MOFs (**BCN-32** and **BCN-33**) via clip-off chemistry (**pcg**). In these syntheses, one of the subnets, particularly the **hxl** net, was removed by quantitatively cleaving the olefinic bonds of the ditopic zigzag linkers of the three-merged net MOFs through ozonolysis. Furthermore, we employed the linker reinstallation approach to revert the formation of the three-merged net MOFs back to the two-merged net MOFs. This approach, allowing for the postsynthetic addition of the **hxl** merged net, was further

https://doi.org/10.1021/jacs.4c15936
J. Am. Chem. Soc. 2025, 147, 1344−1355

utilized to synthesize a fourth isoreticular three-merged net MOF (**BCN-31D**). Notably, most of these transformations occur in a single-crystal-to-single-crystal fashion. Moreover, we have demonstrated that the generation of free carboxylic acid groups after cleaving the olefinic groups can be used to tune the sorption properties of the resulting MOFs, playing a significant role in capturing cationic organic pollutants such as CV and RhB. In summary, these approaches, the merged net, clip-off chemistry, and linker reinstallation, exemplify the rich chemistry available for designing unprecedented MOFs, particularly when linked together (Figure 7).

■ ASSOCIATED CONTENT

Supporting Information

The Supporting Information is available free of charge at https://pubs.acs.org/doi/10.1021/jacs.4c15936.

Detailed experimental section and characterization including PXRD diffractograms, FTIR, NMR, N_2 adsorption, and crystallographic details (PDF)

Accession Codes

CCDC 2368546−2368550 contain the supplementary crystallographic data for this paper. These data can be obtained free of charge via www.ccdc.cam.ac.uk/data_request/cif, or by emailing data_request@ccdc.cam.ac.uk, or by contacting The Cambridge Crystallographic Data Centre, 12 Union Road, Cambridge CB2 1EZ, UK; fax: + 44 1223 336033.

■ AUTHOR INFORMATION

Corresponding Authors

Inhar Imaz − *Catalan Institute of Nanoscience and Nanotechnology (ICN2), CSIC, and Barcelona Institute of Science and Technology, Barcelona 08193, Spain; Departament de Química, Facultat de Ciències, Universitat Autònoma de Barcelona, Bellaterra 08193, Spain;* orcid.org/0000-0002-0278-1141; Email: inhar.imaz@icn2.cat

Daniel Maspoch − *Catalan Institute of Nanoscience and Nanotechnology (ICN2), CSIC, and Barcelona Institute of Science and Technology, Barcelona 08193, Spain; Departament de Química, Facultat de Ciències, Universitat Autònoma de Barcelona, Bellaterra 08193, Spain; ICREA, Barcelona 08010, Spain;* orcid.org/0000-0003-1325-9161; Email: daniel.maspoch@icn2.cat

Authors

Yunhui Yang − *Catalan Institute of Nanoscience and Nanotechnology (ICN2), CSIC, and Barcelona Institute of Science and Technology, Barcelona 08193, Spain; Departament de Química, Facultat de Ciències, Universitat Autònoma de Barcelona, Bellaterra 08193, Spain*

Pilar Fernández-Seriñán − *Catalan Institute of Nanoscience and Nanotechnology (ICN2), CSIC, and Barcelona Institute of Science and Technology, Barcelona 08193, Spain; Departament de Química, Facultat de Ciències, Universitat Autònoma de Barcelona, Bellaterra 08193, Spain;* orcid.org/0000-0002-6456-7386

Borja Ortín-Rubio − *Catalan Institute of Nanoscience and Nanotechnology (ICN2), CSIC, and Barcelona Institute of Science and Technology, Barcelona 08193, Spain; Departament de Química, Facultat de Ciències, Universitat Autònoma de Barcelona, Bellaterra 08193, Spain;* Present Address: Max Planck Institute for Solid State Research, 70569 Stuttgart, Germany; orcid.org/0000-0002-0533-3635

Partha Samanta − *Catalan Institute of Nanoscience and Nanotechnology (ICN2), CSIC, and Barcelona Institute of Science and Technology, Barcelona 08193, Spain; Departament de Química, Facultat de Ciències, Universitat Autònoma de Barcelona, Bellaterra 08193, Spain*

Felipe Gándara − *Materials Science Institute of Madrid (ICMM), Consejo Superior de Investigaciones Científicas (CSIC), Madrid 28049, Spain;* orcid.org/0000-0002-1671-6260

Davide M. Proserpio − *Dipartamento di Chimica, Università degli Studi di Milano, Milano 20133, Italy;* orcid.org/0000-0001-6597-9406

Dongsik Nam − *Catalan Institute of Nanoscience and Nanotechnology (ICN2), CSIC, and Barcelona Institute of Science and Technology, Barcelona 08193, Spain; Departament de Química, Facultat de Ciències, Universitat Autònoma de Barcelona, Bellaterra 08193, Spain;* orcid.org/0000-0002-9941-3504

Judith Juanhuix − *Alba Synchrotron Light Facility, Cerdanyola del Vallès, Barcelona 08290, Spain;* orcid.org/0000-0003-3728-8215

Complete contact information is available at: https://pubs.acs.org/10.1021/jacs.4c15936

Notes

The authors declare no competing financial interest.

■ ACKNOWLEDGMENTS

This work has received funding from the European Union's Horizon 2020 research and innovation program under grant agreement no. 101019003, grant refs. PID2021-124804NB-I00 and PID2021-123287OB-I00 funded by MCIN/AEI/10.13039/501100011033/and by "ERDF A way of making Europe", and the Catalan AGAUR (project 2021 SGR 00458). It was also funded by the CERCA program/Generalitat de Catalunya. ICN2 is supported by the Ochoa Centres of Excellence program, Grant CEX2021-001214-S, funded by MCIN/AEI/10.13039.501100011033. Y.Y. acknowledges the China Scholarship Council for scholarship support. D.N. acknowledges the Juan de la Cierva fellowship from Spanish Ministerio de Ciencia e Innovación. P.S. thanks the Generalitat de Catalunya for a Beatriu de Pinós fellowship (2022 BP 00085) (cofunded by EU under the Marie Skłodowska-Curie Actions grant agreement). D.M.P. thanks the MUR for the grant PRIN2020 "Nature Inspired Crystal Engineering (NICE)" and Prof. Vladislav A. Blatov at the Samara Center for Theoretical Materials Science for providing the free ToposPro software (https://topospro.com).[65]

■ REFERENCES

(1) Yaghi, O. M.; Kalmutzki, M. J.; Diercks, C. S. *Introduction to Reticular Chemistry: Metal-Organic Frameworks and Covalent Organic Frameworks*; John Wiley & Sons, 2019.

(2) Yaghi, O. M. Reticular Chemistry: Molecular Precision in Infinite 2D and 3D. *Mol. Front. J.* **2019**, *03* (01), 66−83.

(3) Cordova, K. E.; Yaghi, O. M. The 'folklore' and reality of reticular chemistry. *Mater. Chem. Front.* **2017**, *1* (7), 1304−1309.

(4) Yaghi, O. M.; O'Keeffe, M.; Ockwig, N. W.; Chae, H. K.; Eddaoudi, M.; Kim, J. Reticular synthesis and the design of new materials. *Nature* **2003**, *423* (6941), 705−714.

(5) Li, M.; Li, D.; O'Keeffe, M.; Yaghi, O. M. Topological Analysis of Metal-Organic Frameworks with Polytopic Linkers and/or Multiple Building Units and the Minimal Transitivity Principle. *Chem. Rev.* **2014**, *114* (2), 1343−1370.
(6) Delgado-Friedrichs, O.; O'Keeffe, M. Three-periodic tilings and nets: face-transitive tilings and edge-transitive nets revisited. *Acta Crystallogr., Sect. A: Found. Crystallogr.* **2007**, *63*, 344−347.
(7) O'Keeffe, M.; Peskov, M. A.; Ramsden, S. J.; Yaghi, O. M. The Reticular Chemistry Structure Resource (RCSR) Database of, and Symbols for, Crystal Nets. *Acc. Chem. Res.* **2008**, *41* (12), 1782−1789.
(8) Guillerm, V.; Eddaoudi, M. The Importance of Highly Connected Building Units in Reticular Chemistry: Thoughtful Design of Metal-Organic Frameworks. *Acc. Chem. Res.* **2021**, *54* (17), 3298−3312.
(9) Jiang, H.; Alezi, D.; Eddaoudi, M. A reticular chemistry guide for the design of periodic solids. *Nat. Rev. Mater.* **2021**, *6* (6), 466−487.
(10) Chen, Z. J.; Weselinski, L. J.; Adil, K.; Belmabkhout, Y.; Shkurenko, A.; Jiang, H.; Bhatt, P. M.; Guillerm, V.; Dauzon, E.; Xue, D. X.; O'Keeffe, M.; Eddaoudi, M. Applying the Power of Reticular Chemistry to Finding the Missing alb-MOF Platform Based on the (6,12)-Coordinated Edge -Transitive Net. *J. Am. Chem. Soc.* **2017**, *139* (8), 3265−3274.
(11) Cavka, J. H.; Jakobsen, S.; Olsbye, U.; Guillou, N.; Lamberti, C.; Bordiga, S.; Lillerud, K. P. A new zirconium inorganic building brick forming metal organic frameworks with exceptional stability. *J. Am. Chem. Soc.* **2008**, *130* (42), 13850−13851.
(12) Xue, D. X.; Cairns, A. J.; Belmabkhout, Y.; Wojtas, L.; Liu, Y. L.; Alkordi, M. H.; Eddaoudi, M. Tunable Rare-Earth fcu-MOFs: A Platform for Systematic Enhancement of CO2 Adsorption Energetics and Uptake. *J. Am. Chem. Soc.* **2013**, *135* (20), 7660−7667.
(13) Morris, W.; Volosskiy, B.; Demir, S.; Gándara, F.; McGrier, P. L.; Furukawa, H.; Cascio, D.; Stoddart, J. F.; Yaghi, O. M. Synthesis, Structure, and Metalation of Two New Highly Porous Zirconium Metal-Organic Frameworks. *Inorg. Chem.* **2012**, *51* (12), 6443−6445.
(14) Luebke, R.; Belmabkhout, Y.; Weselinski, L. J.; Cairns, A. J.; Alkordi, M.; Norton, G.; Wojtas, L.; Adil, K.; Eddaoudi, M. Versatile rare earth hexanuclear clusters for the design and synthesis of highly-connected ftw-MOFs. *Chem. Sci.* **2015**, *6* (7), 4095−4102.
(15) Feng, D. W.; Gu, Z. Y.; Chen, Y. P.; Park, J.; Wei, Z. W.; Sun, Y. J.; Bosch, M.; Yuan, S.; Zhou, H. C. A Highly Stable Porphyrinic Zirconium Metal-Organic Framework with shp-a Topology. *J. Am. Chem. Soc.* **2014**, *136* (51), 17714−17717.
(16) AbdulHalim, R. G.; Bhatt, P. M.; Belmabkhout, Y.; Shkurenko, A.; Adil, K.; Barbour, L. J.; Eddaoudi, M. A Fine-Tuned Metal-Organic Framework for Autonomous Indoor Moisture Control. *J. Am. Chem. Soc.* **2017**, *139* (31), 10715−10722.
(17) Furukawa, H.; Gándara, F.; Zhang, Y. B.; Jiang, J. C.; Queen, W. L.; Hudson, M. R.; Yaghi, O. M. Water Adsorption in Porous Metal-Organic Frameworks and Related Materials. *J. Am. Chem. Soc.* **2014**, *136* (11), 4369−4381.
(18) Feng, L.; Wang, Y. T.; Zhang, K.; Wang, K. Y.; Fan, W. D.; Wang, X. K.; Powell, J. A.; Guo, B. B.; Dai, F. N.; Zhang, L. L.; Wang, R. M.; Sun, D. F.; Zhou, H. C. Molecular Pivot-Hinge Installation to Evolve Topology in Rare-Earth Metal-Organic Frameworks. *Angew. Chem., Int. Ed.* **2019**, *58* (46), 16682−16690.
(19) Chen, Z. J.; Li, P. H.; Wang, X. J.; Otake, K. I.; Zhang, X.; Robison, L.; Atilgan, A.; Islamoglu, T.; Hall, M. G.; Peterson, G. W.; Stoddart, J. F.; Farha, O. K. Ligand-Directed Reticular Synthesis of Catalytically Active Missing Zirconium-Based Metal-Organic Frameworks. *J. Am. Chem. Soc.* **2019**, *141* (31), 12229−12235.
(20) Froudas, K. G.; Vassaki, M.; Papadopoulos, K.; Tsangarakis, C.; Chen, X.; Shepard, W.; Fairen-Jimenez, D.; Tampaxis, C.; Charalambopoulou, G.; Steriotis, T. A.; Trikalitis, P. N. Expanding the Reticular Chemistry Building Block Library toward Highly Connected Nets: Ultraporous MOFs Based on 18-Connected Ternary, Trigonal Prismatic Superpolyhedra. *J. Am. Chem. Soc.* **2024**, *146* (13), 8961−8970.
(21) Guillerm, V.; Kim, D.; Eubank, J. F.; Luebke, R.; Liu, X.; Adil, K.; Lah, M. S.; Eddaoudi, M. A supermolecular building approach for the design and construction of metal-organic frameworks. *Chem. Soc. Rev.* **2014**, *43* (16), 6141−6172.
(22) Nouar, F.; Eubank, J. F.; Bousquet, T.; Wojtas, L.; Zaworotko, M. J.; Eddaoudi, M. Supermolecular building blocks (SBBs) for the design and synthesis of highly porous metal-organic frameworks. *J. Am. Chem. Soc.* **2008**, *130* (6), 1833−1835.
(23) Guillerm, V.; Weselinski, L. J.; Belmabkhout, Y.; Cairns, A. J.; D'Elia, V.; Wojtas, L.; Adil, K.; Eddaoudi, M. Discovery and introduction of a (3,18)-connected net as an ideal blueprint for the design of metal-organic frameworks. *Nat. Chem.* **2014**, *6* (8), 673−680.
(24) Lee, J.; Park, D.; Jin, E.; Lee, S.; Lee, J.; Oh, H.; Choe, W. Programmable Merged-Net Porphyrinic Metal−Organic Frameworks for Water Sorption. *Adv. Funct. Mater.* **2024**, 2413200.
(25) Fang, P. H.; Xing, K.; Qu, L. L.; Ma, Z. S.; Zhou, K.; Liu, X. Y. Reticular Chemistry and In Situ "One-Pot" Strategy: A Dream Combination to Construct Metal−Organic Frameworks. *Small* **2024**, *20*, 2405540.
(26) Yang, N.; Li, H. X.; Ritter, L.; Du, G. T.; Guo, X. A.; Space, B.; Xue, D. X. A Propeller-Like Ligand-Directed Construction of a Tetranuclear Cerium-Organic Framework for Single-Step Ethylene Purification from Ternary C2Mixtures. *Inorg. Chem.* **2024**, *63* (31), 14755−14760.
(27) Jiang, H.; Benzaria, S.; Alsadun, N.; Jia, J.; Czaban-Jóźwiak, J.; Guillerm, V.; Shkurenko, A.; Thiam, Z.; Bonneau, M.; Maka, V. K.; Chen, Z.; Ameur, Z. O.; O'Keeffe, M.; Eddaoudi, M. Merged-nets enumeration for the systematic design of multicomponent reticular structures. *Science* **2024**, *386* (6722), 659−666.
(28) Jiang, H.; Jia, J. T.; Shkurenko, A.; Chen, Z. J.; Adil, K.; Belmabkhout, Y.; Weselinski, L. J.; Assen, A. H.; Xue, D. X.; O'Keeffe, M.; Eddaoudi, M. Enriching the Reticular Chemistry Repertoire: Merged Nets Approach for the Rational Design of Intricate Mixed-Linker Metal-Organic Framework Platforms. *J. Am. Chem. Soc.* **2018**, *140* (28), 8858−8867.
(29) Jiang, H.; Moosavi, S. M.; Czaban-Józwiak, J.; Torre, B.; Shkurenko, A.; Ameur, Z. O.; Jia, J. T.; Alsadun, N.; Shekhah, O.; Di Fabrizio, E.; Smit, B.; Eddaoudi, M. Reticular chemistry for the rational design of mechanically robust mesoporous merged-net metal-organic frameworks. *Matter* **2023**, *6* (1), 285−295.
(30) Fang, H.; Zheng, B.; Zhang, Z. H.; Li, H. X.; Xue, D. X.; Bai, J. F. Ligand-Conformer-Induced Formation of Zirconium-Organic Framework for Methane Storage and MTO Product Separation. *Angew. Chem., Int. Ed.* **2021**, *60* (30), 16521−16528.
(31) Yang, Y. H.; Broto-Ribas, A.; Ortín-Rubio, B.; Imaz, I.; Gándara, F.; Carné-Sánchez, A.; Guillerm, V.; Jurado, S.; Busqué, F.; Juanhuix, J.; Maspoch, D. Clip-off Chemistry: Synthesis by Programmed Disassembly of Reticular Materials. *Angew. Chem., Int. Ed.* **2022**, *61* (4), No. e202111228.
(32) Yang, Y. H.; Fernández-Seriñán, P.; Imaz, I.; Gándara, F.; Handke, M.; Ortín-Rubio, B.; Juanhuix, J.; Maspoch, D. Isoreticular Contraction of Metal-Organic Frameworks Induced by Cleavage of Covalent Bonds. *J. Am. Chem. Soc.* **2023**, *145* (31), 17398−17405.
(33) Broto-Ribas, A.; Ruiz-Relaño, S.; Albalad, J.; Yang, Y.; Gándara, F.; Juanhuix, J.; Imaz, I.; Maspoch, D. Retrosynthetic Analysis Applied to Clip-off Chemistry: Synthesis of Four Rh(II)-Based Complexes as Proof-of-Concept. *Angew. Chem., Int. Ed.* **2023**, *62*, No. e202310354.
(34) Nam, D.; Albalad, J.; Sánchez-Naya, R.; Ruiz-Relaño, S.; Cortés-Martínez, A.; Yang, Y.; Juanhuix, J.; Imaz, I.; Maspoch, D. Isolation of the Secondary Building Unit of a 3D Metal−Organic Framework through Clip-Off Chemistry, and Its Reuse To Synthesize New Frameworks by Dynamic Covalent Chemistry. *J. Am. Chem. Soc.* **2024**, *146* (40), 27255−27261.
(35) Ruiz-Relaño, S.; Nam, D.; Albalad, J.; Cortés-Martínez, A.; Juanhuix, J.; Imaz, I.; Maspoch, D. Synthesis of Metal−Organic Cages via Orthogonal Bond Cleavage in 3D Metal−Organic Frameworks. *J. Am. Chem. Soc.* **2024**, *146* (39), 26603−26608.
(36) Nishijima, A.; Osugi, Y.; Uemura, T. Fabrication of Self-Expanding Metal−Organic Cages Using a Ring-Openable Ligand. *Angew. Chem., Int. Ed.* **2024**, *63*, No. e202404155.

https://doi.org/10.1021/jacs.4c15936
J. Am. Chem. Soc. 2025, 147, 1344−1355

(37) Schoedel, A.; Zaworotko, M. J. [M3(μ3-O)(O2CR)6] and related trigonal prisms: versatile molecular building blocks for crystal engineering of metal-organic material platforms. *Chem. Sci.* **2014**, *5* (4), 1269−1282.
(38) Chen, W. M.; Wang, Z.; Wang, Q.; El-Yanboui, K.; Tan, K.; Barkholtz, H. M.; Liu, D. J.; Cai, P. Y.; Feng, L.; Li, Y. C.; Qin, J. S.; Yuan, S.; Sun, D.; Zhou, H. C. Monitoring the Activation of Open Metal Sites in [FeXM3-X(μ3-O)] Cluster-Based Metal-Organic Frameworks by Single-Crystal X-ray Diffraction. *J. Am. Chem. Soc.* **2023**, *145* (8), 4736−4745.
(39) Wang, X. K.; Xu, M. M.; Fan, W. D.; Sun, D. F. Fe-Based Metal-Organic Frameworks: From Various Synthesis, Diverse Structures to Multifunctional Applications. *Chin. J. Chem.* **2023**, *41* (24), 3772−3791.
(40) Férey, G.; Mellot-Draznieks, C.; Serre, C.; Millange, F.; Dutour, J.; Surblé, S.; Margiolaki, I. A chromium terephthalate-based solid with unusually large pore volumes and surface area. *Science* **2005**, *309* (5743), 2040−2042.
(41) Serre, C.; Millange, F.; Surblé, S.; Férey, G. A route to the synthesis of trivalent transition-metal porous carboxylates with trimeric secondary building units. *Angew. Chem., Int. Ed.* **2004**, *43* (46), 6285−6289.
(42) Férey, G.; Serre, C.; Mellot-Draznieks, C.; Millange, F.; Surblé, S.; Dutour, J.; Margiolaki, I. A hybrid solid with giant pores prepared by a combination of targeted chemistry, simulation, and powder diffraction. *Angew. Chem., Int. Ed.* **2004**, *43* (46), 6296−6301.
(43) Reinares-Fisac, D.; Aguirre-Díaz, L. M.; Iglesias, M.; Snejko, N.; Gutiérrez-Puebla, E.; Monge, M. A.; Gándara, F. A Mesoporous Indium Metal-Organic Framework: Remarkable Advances in Catalytic Activity for Strecker Reaction of Ketones. *J. Am. Chem. Soc.* **2016**, *138* (29), 9089−9092.
(44) Feng, D. W.; Wang, K. C.; Wei, Z. W.; Chen, Y. P.; Simon, C. M.; Arvapally, R. K.; Martin, R. L.; Bosch, M.; Liu, T. F.; Fordham, S.; Yuan, D. Q.; Omary, M. A.; Haranczyk, M.; Smit, B.; Zhou, H. C. Kinetically tuned dimensional augmentation as a versatile synthetic route towards robust metal-organic frameworks. *Nat. Commun.* **2014**, *5*, 5723.
(45) Chevreau, H.; Devic, T.; Salles, F.; Maurin, G.; Stock, N.; Serre, C. Mixed-Linker Hybrid Superpolyhedra for the Production of a Series of Large-Pore Iron(III) Carboxylate Metal-Organic Frameworks. *Angew. Chem., Int. Ed.* **2013**, *52* (19), 5056−5060.
(46) Nguyen, T. T. M.; Le, H. M.; Kawazoe, Y.; Nguyen, H. L. Reticular control of interpenetration in a complex metal-organic framework. *Mater. Chem. Front.* **2018**, *2* (11), 2063−2069.
(47) Prasad, R. R. R.; Pleass, C.; Rigg, A. L.; Cordes, D. B.; Lozinska, M. M.; Georgieva, V. M.; Hoffmann, F.; Slawin, A. M. Z.; Wright, P. A. Isoreticular chemistry of scandium analogues of the multicomponent metal-organic framework MIL-142. *CrystEngComm* **2021**, *23* (4), 804−812.
(48) Nguyen, H. L.; Vu, T. T.; Nguyen, D. K.; Trickett, C. A.; Doan, T. L. H.; Diercks, C. S.; Nguyen, V. Q.; Cordova, K. E. A complex metal-organic framework catalyst for microwave-assisted radical polymerization. *Commun. Chem.* **2018**, *1* (1), 70.
(49) Guillerm, V.; Maspoch, D. Geometry Mismatch and Reticular Chemistry: Strategies To Assemble Metal-Organic Frameworks with Non-default Topologies. *J. Am. Chem. Soc.* **2019**, *141* (42), 16517−16538.
(50) Guillerm, V.; Grancha, T.; Imaz, I.; Juanhuix, J.; Maspoch, D. Zigzag Ligands for Transversal Design in Reticular Chemistry: Unveiling New Structural Opportunities for Metal-Organic Frameworks. *J. Am. Chem. Soc.* **2018**, *140* (32), 10153−10157.
(51) **fka** *net in Reticular Chemistry Structure Resource (RCSR) database*. http://rcsr.net/nets/fka (accessed 2024−11−08).
(52) **pcg** *net in Reticular Chemistry Structure Resource (RCSR) database*. http://rcsr.net/nets/pcg (accessed 2024−11−08).
(53) Feng, L.; Yuan, S.; Qin, J. S.; Wang, Y.; Kirchon, A.; Qiu, D.; Cheng, L.; Madrahimov, S. T.; Zhou, H. C. Lattice Expansion and Contraction in Metal-Organic Frameworks by Sequential Linker Reinstallation. *Matter* **2019**, *1* (1), 156−167.
(54) Hu, Y. C.; Zhang, X.; Khoo, R. S. H.; Fiankor, C.; Zhang, X.; Zhang, J. Stepwise Assembly of Quinary Multivariate Metal-Organic Frameworks via Diversified Linker Exchange and Installation. *J. Am. Chem. Soc.* **2023**, *145* (25), 13929−13937.
(55) Zhang, X.; Frey, B. L.; Chen, Y. S.; Zhang, J. Topology-Guided Stepwise Insertion of Three Secondary Linkers in Zirconium Metal-Organic Frameworks. *J. Am. Chem. Soc.* **2018**, *140* (24), 7710−7715.
(56) Yuan, S.; Chen, Y. P.; Qin, J. S.; Lu, W. G.; Zou, L. F.; Zhang, Q.; Wang, X.; Sun, X.; Zhou, H. C. Linker Installation: Engineering Pore Environment with Precisely Placed Functionalities in Zirconium MOFs. *J. Am. Chem. Soc.* **2016**, *138* (28), 8912−8919.
(57) Chen, Y. W.; Idrees, K. B.; Mian, M. R.; Son, F. A.; Zhang, C. H.; Wang, X. J.; Farha, O. K. Reticular Design of Precise Linker Installation into a Zirconium Metal-Organic Framework to Reinforce Hydrolytic Stability. *J. Am. Chem. Soc.* **2023**, *145* (5), 3055−3063.
(58) Chen, Y. W.; Xie, H. M.; Zhong, Y. H.; Sha, F. R.; Kirlikovali, K. O.; Wang, X. L.; Zhang, C. H.; Li, Z. B.; Farha, O. K. Programmable Water Sorption through Linker Installation into a Zirconium Metal-Organic Framework. *J. Am. Chem. Soc.* **2024**, *146* (16), 11202−11210.
(59) Tu, B.; Pang, Q.; Wu, D.; Song, Y.; Weng, L.; Li, Q. Ordered Vacancies and Their Chemistry in Metal−Organic Frameworks. *J. Am. Chem. Soc.* **2014**, *136* (41), 14465−14471.
(60) Yuan, S.; Zhang, P.; Zhang, L.; Garcia-Esparza, A. T.; Sokaras, D.; Qin, J. S.; Feng, L.; Day, G. S.; Chen, W.; Drake, H. F.; Elumalai, P.; Madrahimov, S. T.; Sun, D.; Zhou, H. C. Exposed Equatorial Positions of Metal Centers via Sequential Ligand Elimination and Installation in MOFs. *J. Am. Chem. Soc.* **2018**, *140* (34), 10814−10819.
(61) *Materials Studio*, ver. 7.0; Accelrys Inc.: San Diego, CA.
(62) Bhadra, B. N.; Ahmed, I.; Lee, H. J.; Jhung, S. H. Metal-organic frameworks bearing free carboxylic acids: Preparation, modification, and applications. *Coord. Chem. Rev.* **2022**, *450*, No. 214237.
(63) Zhang, W.; Yang, J. M.; Yang, R. N.; Yang, B. C.; Quan, S.; Jiang, X. Effect of free carboxylic acid groups in UiO-66 analogues on the adsorption of dyes from water: Plausible mechanisms for adsorption and gate-opening behavior. *J. Mol. Liq.* **2019**, *283*, 160−166.
(64) Gao, X.; Zheng, M.; Zhao, X.; Song, S.; Gao, Z. Ultra-High-Capacity Adsorption of Rhodamine B in a Carboxyl-Functionalized Metal−Organic Framework via Surface Adsorption. *J. Chem. Eng. Data* **2021**, *66*, 669−676.
(65) Blatov, V. A.; Shevchenko, A. P.; Proserpio, D. M. Applied Topological Analysis of Crystal Structures with the Program Package ToposPro. *Cryst. Growth Des.* **2014**, *14* (7), 3576−3586.

https://doi.org/10.1021/jacs.4c15936
J. Am. Chem. Soc. 2025, 147, 1344−1355